Frontiers in Bioscience Landmark

Front. Biosci. (Landmark Ed) **2026**; 31(9): 53591
https://doi.org/10.31083/FBL53591

Original Research

Arhgap25 Promotes Metabolic Dysfunction-Associated Steatotic Liver Disease (MASLD) by Driving Kupffer Cell Polarization via Activation of the AKT/mTOR Signaling Pathway

Yan Wang[1], Shuangshuang Lu[2,*]

[1]Department of Gastroenterology, The First Affiliated Hospital of Zhengzhou University, 450052 Zhengzhou, Henan, China
[2]School of Basic Medical Sciences, Zhengzhou University, 450052 Zhengzhou, Henan, China
*Correspondence: Lushuangshuang@zzu.edu.cn (Shuangshuang Lu)

Academic Editor: Guor Mour Her
Submitted: 6 May 2026 Revised: 11 July 2026 Accepted: 23 July 2026 Published: 7 September 2026

Abstract

Background: Metabolic dysfunction-associated steatotic liver disease (MASLD) is a leading global health burden, yet the regulatory nodes linking hepatic immune dysregulation to metabolic perturbations remain incompletely understood. **Methods:** We integrated bulk and single-cell RNA sequencing (scRNA-seq) to identify core regulatory genes dysregulated by a high-fat diet (HFD). The functional role of the candidate gene Arhgap25, was validated using an adeno-associated virus (AAV)-mediated overexpression mouse model and an *in vitro* Kupffer cell (KC)-hepatocyte co-culture system. **Results:** Integrated transcriptomic analysis identified Arhgap25 as a key differentially expressed gene consistently upregulated in HFD-fed livers, with specific enrichment in KCs. *In vivo*, Arhgap25 overexpression significantly promoted macrovesicular steatosis, increased intrahepatic triglycerides and cholesterol levels, and exacerbated liver injury. Mechanistically, Arhgap25 triggered a pro-inflammatory microenvironment by promoting KC polarization toward the M1 phenotype, characterized by increased TNF-α, IL-6, and IL-1β expression and suppression of the M2 marker ARG1. *In vitro* co-culture assays demonstrated that Arhgap25 exacerbated hepatocellular lipid accumulation and inflammatory responses by promoting the phosphorylation of the AKT/mTOR signaling axis. AKT inhibition further confirmed this signaling dependency. **Conclusion:** Our findings establish Arhgap25 as a critical mediator in the hepatic immune-metabolic network. By positively regulating AKT/mTOR signaling in KCs, Arhgap25 promotes M1 polarization and subsequent metabolic dysfunction, highlighting it as a potential therapeutic target for MASLD.

Keywords: fatty liver; ARHGAP25; Kupffer cells; AKT/mTOR signaling pathway

1. Introduction

Metabolic dysfunction-associated steatotic liver disease (MASLD) has emerged as the most prevalent chronic liver disease worldwide, imposing a profound clinical and economic burden globally [1,2,3]. The etiology and progression of MASLD are intrinsically linked to high-fat diet (HFD) consumption and systemic obesity [4,5]. This pathological cascade typically begins with the excessive hepatic accumulation of free fatty acids (FFAs) and triglycerides (TGs), which can subsequently progress to steatohepatitis—characterized by hepatocellular injury—and ultimately culminate in liver fibrosis or hepatocellular carcinoma [6]. Within this complex disease continuum, it is increasingly recognized that lipid dysregulation alone is insufficient to fully elucidate progressive hepatic deterioration of the liver. Emerging evidence indicates that the pathological crosstalk between hepatic parenchymal cells and the local immune microenvironment, particularly the dysregulation of immune networks, serves as a core driver in the transition from isolated steatosis to an advanced inflammatory state.

As the most abundant resident innate immune cells in the liver, Kupffer cells (KCs) function as both sentinels and central regulators of hepatic immune homeostasis and local metabolic equilibrium [7,8]. Studies have shown that activating G protein-coupled receptor 3 (GPR3) in Kupffer cells promotes glycolysis and protects mice against obesity and fatty liver disease [9]. Furthermore, in the context of MASLD, inducing TFEB expression enhances the adaptive capacity of Kupffer cells, helping to alleviate hepatic steatosis [10]. Specifically, this stress drives KCs polarization from a reparative, anti-inflammatory phenotype (M2) toward a highly cytotoxic, pro-inflammatory phenotype (M1) state [11]. This M1 polarization is characterized by the robust secretion of chemokines and pro-inflammatory cytokines, such as TNF-α and IL-6, which not only amplify the local inflammatory cascade but also directly exacerbate hepatocellular lipid accumulation and apoptosis [12,13]. Although the critical role of macrophage polarization in metabolic liver diseases is widely acknowledged, the precise regulatory mechanisms governing KC activation and coupling immune-inflammatory responses to lipid metabolic perturbations remain incompletely elucidated.

Arhgap25 (Rho GTPase activating protein 25) represents a promising candidate for mediating the immune-metabolic crosstalk. Arhgap25 is a negative regulator predominantly expressed in the hematopoietic system and immune cells [14,15,16]. It inactivates small GTPases such as Rac, thereby regulating glycolysis, leukocyte migration, phagocytosis, and superoxide production [15,16,17,18]. Although Arhgap25 modulates local inflammatory responses in various immune-mediated diseases, its role in hepatic immune microenvironment remodeling and obesity-induced lipid dysregulation remains largely unexplored.

To elucidate robust transcriptional signatures and identify core regulatory factors induced by HFD, we conducted a comprehensive comparative analysis of three independent transcriptomic datasets (GSE262523, GSE292565, and GSE263975) [19,20,21]. Our analysis identified 53 differentially expressed genes (DEGs) that were consistently regulated across multiple cohorts. Functional enrichment revealed that these DEGs are predominantly associated with immune responses and myeloid leukocyte-mediated inflammation. Notably, *Arhgap25* was significantly upregulated across all HFD cohorts. Furthermore, single-cell RNA sequencing (scRNA-seq) analysis revealed profound remodeling of the hepatic immune microenvironment following high-fat consumption, characterized by the significant expansion of KC and T cell populations. Within these immune subpopulations, *Arhgap25* was significantly upregulated specifically enriched in KCs.

Building upon these multi-omics findings, the present study aimed to delineate the precise role of Arhgap25 in the pathological progression of MASLD. Using an AAV-mediated *in vivo* overexpression (OE) model, we demonstrated that Arhgap25 significantly promoted macrovesicular steatosis, exacerbating hepatic lipid accumulation and liver injury. Concurrently, Arhgap25 induced a robust pro-inflammatory state, promoting M1 macrophage polarization accompanied by the robust secretion of pro-inflammatory cytokines. *In vitro* co-culture models of KCs and hepatocytes further confirmed that Arhgap25 exerts its pro-lipogenic and pro-inflammatory effects by promote the AKT/mTOR signaling pathway. Collectively, this study not only provides novel mechanistic insights into immune-mediated metabolic dysfunction and highlights Arhgap25 as a critical mediator in the hepatic immune-metabolic network, offering a promising interdisciplinary therapeutic target for obesity-associated metabolic liver diseases.

2. Materials and Methods

2.1 Animals and Diets

Seven-week-old male C57BL/6 mice were obtained from Vital River Laboratory Animal Technology Co., Ltd. (Beijing, China). All animals were housed in a temperature-controlled facility under a standard 12-hour light/dark cycle with ad libitum access to food and water. Following acclimatization, the mice were randomly assigned to two cohorts (n = 6 per group). To establish the overexpression model, mice received a single tail vein injection of 5×10^8 plaque-forming units (PFU) of either AAV-Arhgap25 (OE group) or control AAV-GFP (NC group).

Following injection, all mice were maintained on a Clinton-Cybulsky high-fat diet containing 60% fat (Cat# TP23400; Trophic Animal Feed High-Tech Co., Ltd., Nantong, Jiangsu, China). At the end of the experimental period, the mice were euthanized via an intraperitoneal injection of 5% pentobarbital sodium (150 mg/kg body weight).

2.2 Cell Culture

Human hepatoma HepG2 cells and the Kupffer cell line were cultured in Dulbecco's Modified Eagle Medium (DMEM) supplemented with 10% fetal bovine serum (FBS), 100 U/mL penicillin, and 100 µg/mL streptomycin. All cell lines were validated by STR profiling and tested negative for mycoplasma. All cells were maintained in a humidified atmosphere incubator at 37 °C with 5% CO_2. To investigate intercellular crosstalk between macrophages and hepatic parenchymal cells, a non-contact *in vitro* co-culture system was established using Transwell inserts with a 0.4-µm pore size. This configuration permits the free exchange of soluble cytokines and metabolites while preventing direct physical contact between the two cell populations. HepG2 cells were seeded in the lower chambers, while Kupffer cells were seeded in the upper Transwell inserts.

To mimic the *in vivo* high-lipid environment and establish an *in vitro* model of hepatocellular lipid accumulation, HepG2 cells in the lower chambers were subjected to palmitic acid (PA) loading. PA was pre-dissolved in 0.1 M NaOH and saponified at 70 °C in a water bath, followed by conjugation with 10% fatty acid-free bovine serum albumin (BSA) to yield a PA-BSA stock solution. For experimental treatments, this stock solution was added to the HepG2 culture medium to a final concentration of 500 µM. Cells were incubated with 500 µM PA for 24 hours to induce substantial intracellular lipid accumulation and a steatotic phenotype. Normal control (NC) cells were treated with an equivalent volume of the fatty acid-free BSA carrier.

2.3 Public Data Acquisition and Bulk RNA-seq Analysis

Three independent transcriptomic datasets (GSE262523, GSE292565, and GSE263975) were obtained from the Gene Expression Omnibus (GEO) database. DEGs between HFD and control groups were identified using the *limma* or *DESeq2* packages in R. Subsequent intersection analysis was conducted to identify consistently dysregulated core DEGs across the all cohorts.

2.4 Single-cell RNA Sequencing (scRNA-seq) and Processing

Hepatic tissues from HFD and Normal Chow Diet (NCD) mice were dissociated into single-cell suspensions. Libraries were constructed and sequenced using the 10x Genomics Chromium platform (10x Genomics, Pleasanton, CA, USA). Raw sequencing data were processed using the *Seurat* package in R for quality control, normalization, and dimensionality reduction. Uniform Manifold Approximation and Projection (UMAP) was employed for the non-linear dimensionality reduction and visualization of cell clusters. Cell types were annotated based on the expression of established canonical marker genes.

2.5 Functional Enrichment and Intercellular Communication

Gene Ontology (GO) biological process enrichment analysis of the core and cluster-specific DEGs was conducted using the *clusterProfiler* package in R. To investigate the intercellular interactions, cell-cell communication analysis was performed and visualized via chord diagrams, highlighting the signaling crosstalk between KCs and other hepatic cell populations.

2.6 Histological Analysis and Biochemical Assays

Following euthanasia, liver tissues were rapidly harvested and partitioned for subsequent analyses. A portion of the liver tissue was fixed in 4% formaldehyde at 4 °C for histological evaluation. Immunofluorescence (IF) and immunohistochemical (IHC) staining were subsequently performed on the fixed tissues using an anti-ADGRE1 primary antibody (1:50, ab16911; Abcam). For lipid visualization, a separate aliquot of the fresh liver tissue was embedded in optimal cutting temperature (OCT) compound and snap-frozen. The frozen tissues were sectioned at a thickness of 10 μm and subjected to Oil Red O and Hematoxylin and Eosin (H&E) staining. To precisely quantify hepatic lipid accumulation, intrahepatic triglyceride (TG) and total cholesterol (TC) levels were measured using commercial colorimetric assay kits (Cat# BC0625 for TG, Cat# BC1985 for TC; Solarbio Life Science, Beijing, China) according to the manufacturer's protocols.

2.7 Western Blot Analysis

Equal amounts of total protein lysates (15 μg per lane) were separated via 10% sodium dodecyl sulfate-polyacrylamide gel electrophoresis (SDS-PAGE) and subsequently transferred onto polyvinylidene fluoride (PVDF) membranes. The membranes were blocked and subsequently probed overnight at 4 °C with the following primary antibodies: anti-β-Actin (Cat# R380624; ZENBIO), anti-Arhgap25 (Cat# A13664; ABclonal), anti-ARG1 (Cat# A1847SP; ABclonal), anti-TNFα (Cat# 346654; ZENBIO), anti-IL1β (Cat# 660092; ZENBIO), anti-CD68 (Cat# 360018; ZENBIO), anti-IL6 (Cat# A27935; ABclonal), anti-PPARγ (Cat# 340844; ZENBIO), anti-FABP4 (Cat# R381753; ZENBIO), anti-CEBPβ (Cat# R380893; ZENBIO), anti-AKT (Cat# 9272; CST), anti-p-AKT (Cat# 4060; CST), anti-mTOR (Cat# 2972; CST), and anti-p-mTOR (Cat# 2971; CST). Following incubation with the appropriate secondary antibodies, protein bands were visualized using enhanced chemiluminescence (ECL), and densitometric quantification was performed using ImageJ software 1.54f (National Institutes of Health, Bethesda, MD, USA). All experiments were performed in triplicate. All primary antibodies used in this study are detailed in **Supplementary Table 1**.

2.8 BODIPY Staining for Lipid Droplets

Intracellular lipid droplet accumulation was evaluated using a Lipid Droplets Green Fluorescence Assay Kit with BODIPY 493/503 (Cat# C2053S; Beyotime Biotechnology, Shanghai, China). Following an 8-day culture and specified induction period in 24-well plates, hepatocytes cultured in 24-well plates were fixed with 4% paraformaldehyde (PFA) for 60 minutes at room temperature. After washing twice with phosphate-buffered saline (PBS), the cells were incubated with 250 μL of BODIPY staining solution per well for 10–20 minutes at room temperature in the dark, in strict accordance with the manufacturer's protocol. Subsequently, the cells were washed three times with PBS to remove excess dye. Fluorescently labeled lipid droplets were imaged using an Olympus IX71 fluorescence microscope (Olympus, Tokyo, Japan) at an excitation wavelength of 488 nm.

2.9 RNA Isolation and Quantitative Real-Time PCR (RT-qPCR)

Total RNA was extracted from tissue and cell samples using the RNAiso Plus reagent (Cat# 9109; Takara Bio Inc., Beijing, China) in strict accordance with the manufacturer's instructions. Subsequently, 500 ng of total RNA per sample was reverse-transcribed into complementary DNA (cDNA) using the PrimeScript™ RT Master Mix (Perfect Real Time) (Cat# RR036A; Takara Bio Inc.). Quantitative real-time PCR (qPCR) amplification was performed using the ChamQ SYBR qPCR Master Mix (Cat# Q311-02; Vazyme, Nanjing, Jiangsu, China) on an ABI StepOne Plus system. The relative mRNA expression levels were calculated using the $2^{-\Delta\Delta Ct}$ method and normalized to β-actin. All specific primer sequences used in this study are detailed in **Supplementary Table 2**.

2.10 Statistical Analysis

All *in vitro* and *in vivo* experiments were performed in at least three independent biological replicates. Animals were randomly assigned to experimental groups using a computer-generated random number sequence. To minimize systematic bias, cell culture plates and tissue samples were processed and analyzed in a randomized order. All

statistical analyses were conducted using SPSS software, version 23.0 (SPSS Inc., Chicago, IL, USA).

Data are presented as the mean ± standard error of the mean (SEM), with scatter plots illustrating individual data points. The normality of the data distribution was assessed using the Shapiro-Wilk test. For normally distributed data, statistical comparisons between two independent groups were analyzed using an unpaired two-tailed Student's *t*-test. Differences among three or more groups were analyzed using a one-way analysis of variance (ANOVA) followed by Tukey's post hoc test for multiple comparisons. A p-value < 0.05 was considered statistically significant.

3. Results

3.1 Identification of Core DEGs Across Multiple Datasets

To identify robust transcriptional signatures associated with HFD induced changes, we performed a comparative analysis of three independent transcriptomic datasets: GSE262523, GSE292565, and GSE263975. Intersection of these datasets identified 53 DEGs consistently regulated across all three cohorts (Fig. 1A). Among these core genes, *Arhgap25* emerged as a prominent candidate, alongside other immune-related markers such as *Adam8*, *Cd68*, and *Cd52*. To elucidate the biological significance of these 53 DEGs, we performed Gene Ontology Biological Process enrichment analysis. The results demonstrated that these genes are predominantly involved in immune responses and leukocyte dynamics (Fig. 1B). The most significantly enriched pathways included myeloid leukocyte migration, leukocyte chemotaxis, and positive regulation of cell activation, suggesting that the HFD-induced transcriptional response is heavily driven by myeloid-mediated inflammation. Volcano plot analysis confirmed that *Arhgap25* was significantly upregulated in the HFD groups compared to controls across all three cohorts (GSE263975, GSE262523, and GSE292565; Fig. 1C). The consistent upregulation of *Arhgap25* across these independent cohorts suggests its potential role as a key regulator in HFD-induced pathology.

To characterize the hepatic cellular heterogeneity under metabolic stress, we performed scRNA-seq on liver samples from HFD- and NCD-fed groups. UMAP visualization identified distinct clusters representing major hepatic and immune cell populations, including hepatocytes, KCs, macrophages, LSECs, T cells, and neutrophils (Fig. 1D). The identities of these clusters were validated using established cell-type-specific marker genes, as shown in the dot plot (Fig. 1E). Quantitative analysis of cell-type proportions revealed shifts in the cellular composition between the two groups. Specifically, the HFD group exhibited a marked increase in the proportions of KCs and T cells, accompanied by a relative depletion of LSECs compared to the NCD group (Fig. 1F). These shifts indicate a profound remodeling of the hepatic immune microenvironment in response to HFD consumption.

3.2 Cell-Type Specific Expression and Functional Profiling of Arhgap25

To further investigate the cellular source of *Arhgap25*, we analyzed its expression across the various cell populations identified by scRNA-seq. *Arhgap25* exhibited significant upregulation in several immune cell clusters under HFD conditions, most notably in KCs (Fig. 2A). Focusing on KCs, we performed GO enrichment analysis to elucidate the functional implications of HFD-induced transcriptional changes. Upregulated genes in the HFD group were primarily enriched in metabolic and energy-related processes, including oxidative phosphorylation and ATP synthesis (Fig. 2B). Conversely, downregulated genes were associated with cell migration and circadian rhythm regulation (Fig. 2C). Furthermore, cell-cell communication analysis (Chord diagram) revealed robust interactions between KCs and other lineages, particularly hepatocytes and LSECs, highlighting the central role of KCs within the hepatic niche (Fig. 2D).

To validate these bioinformatic findings, we performed qPCR and Western blot analysis on liver tissues. Consistent with the sequencing data, *Arhgap25* mRNA levels were significantly elevated in the HFD group compared to the control NCD group (Fig. 2E). Cell-type-specific qPCR further confirmed that *Arhgap25* expression was significantly higher in KCs than in Hepatocytes (Fig. 2E). Furthermore, analysis of the human fatty liver dataset GSE281797—comprising 94 subjects categorized as healthy, MASL (metabolic dysfunction-associated steatotic liver), or MASH (metabolic dysfunction-associated steatohepatitis)—revealed that ARHGAP25 expression was significantly elevated in MASL and MASH patients, mirroring the expression trend observed in the murine models (Fig. 2F). Finally, Western blot analysis demonstrated a marked increase in Arhgap25 protein expression levels in HFD-fed mouse liver (Fig. 2G). Collectively, these results confirm that Arhgap25 is significantly induced by an HFD, particularly within the KC population.

3.3 Arhgap25 Promotes Hepatic Lipid Accumulation

To evaluate the impact of Arhgap25 on hepatic lipid accumulation and liver injury, we established AAV-mediated overexpression (OE) mouse model. Histological evaluation via H&E and Oil Red O staining revealed substantial macrovesicular steatosis and increased lipid droplet accumulation in the liver tissues of the OE group compared to the NC group (Fig. 3A). The relative mRNA expression levels of adipogenic transcription factors and fatty acid-binding proteins, including PPARγ, *C/EBPβ*, and *FABP4*, were significantly upregulated in the OE group ($p < 0.01$). While *HSL* expression also exhibited a significant increase ($p < 0.05$), *ATGL* expression showed no significant difference between the two groups (Fig. 3B). Consistent with the morphological observations, quantitative biochemical

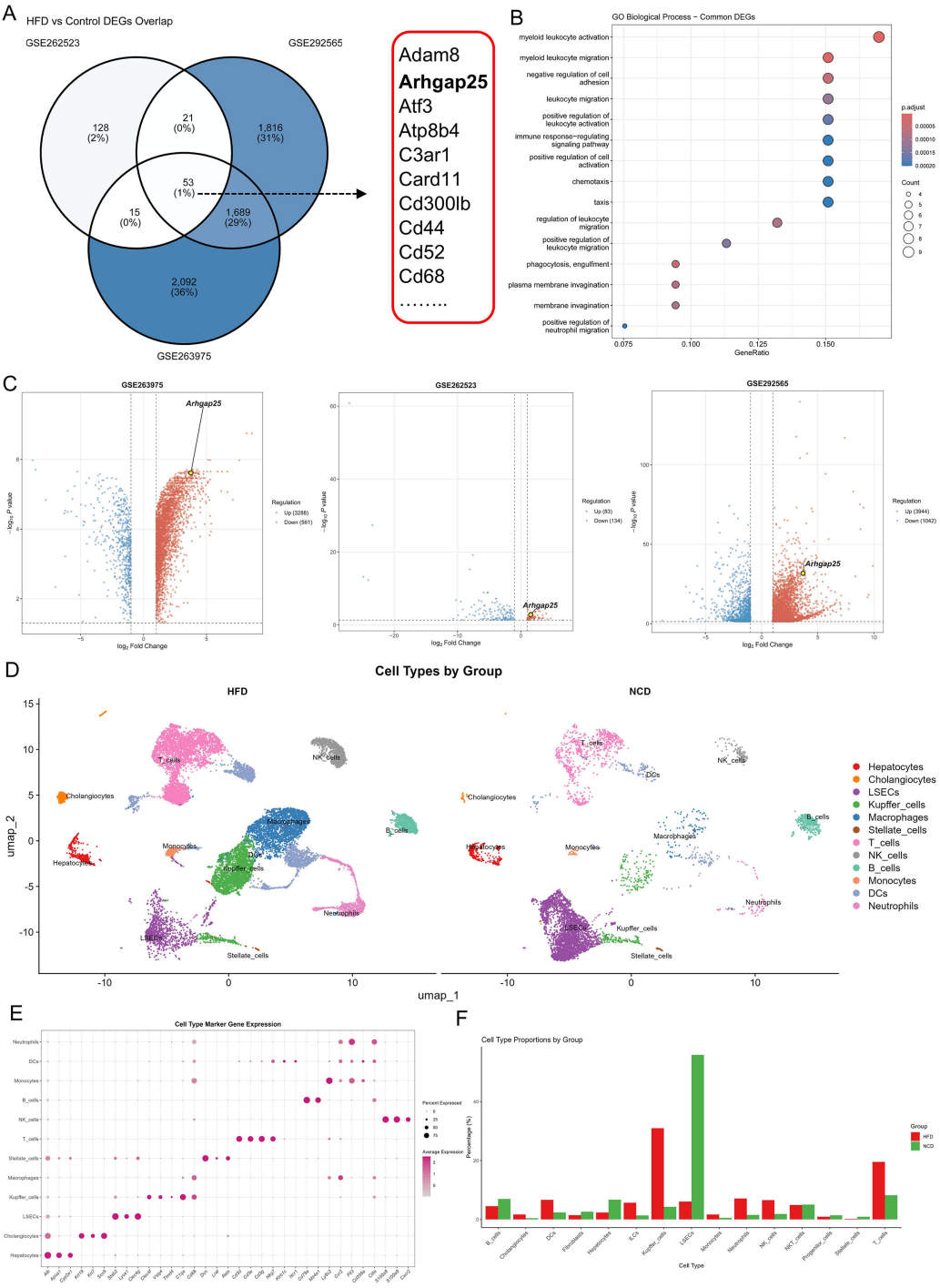

Fig. 1. Bioinformatic identification and single-cell characterization of HFD-induced transcriptional signatures. (A) Venn diagram illustrating the intersection of 53 conserved DEGs across three independent HFD datasets. The boxed region highlights core candidates including *Arhgap25*. (B) Top Gene Ontology biological processes enriched among the common DEGs, predominantly related to myeloid leukocyte migration and activation. (C) Volcano plots depicting the differential expression profiles of GSE263975, GSE262523, and GSE292565 (in this dataset, the conversion of raw data to Gene IDs resulted in a loss of information, leading to inconsistencies in the number of DEGs shown in the volcano plot and Venn diagram), highlighting the consistent upregulation of *Arhgap25*. (D) UMAP visualization of hepatic single-cell landscape in the HFD and NCD groups. (E) Dot plot displaying the canonical markers used to define each cell cluster. Node color and size represent relative expression intensity and cell percentage, respectively. (F) Comparison of relative cell-type frequencies between groups, highlighting HFD-induced shifts in the KC and T-cell populations. HFD, high-fat diet; DEGs, differentially expressed genes; GO, Gene Ontology; NCD, Normal Chow Diet; KC, Kupffer cell.

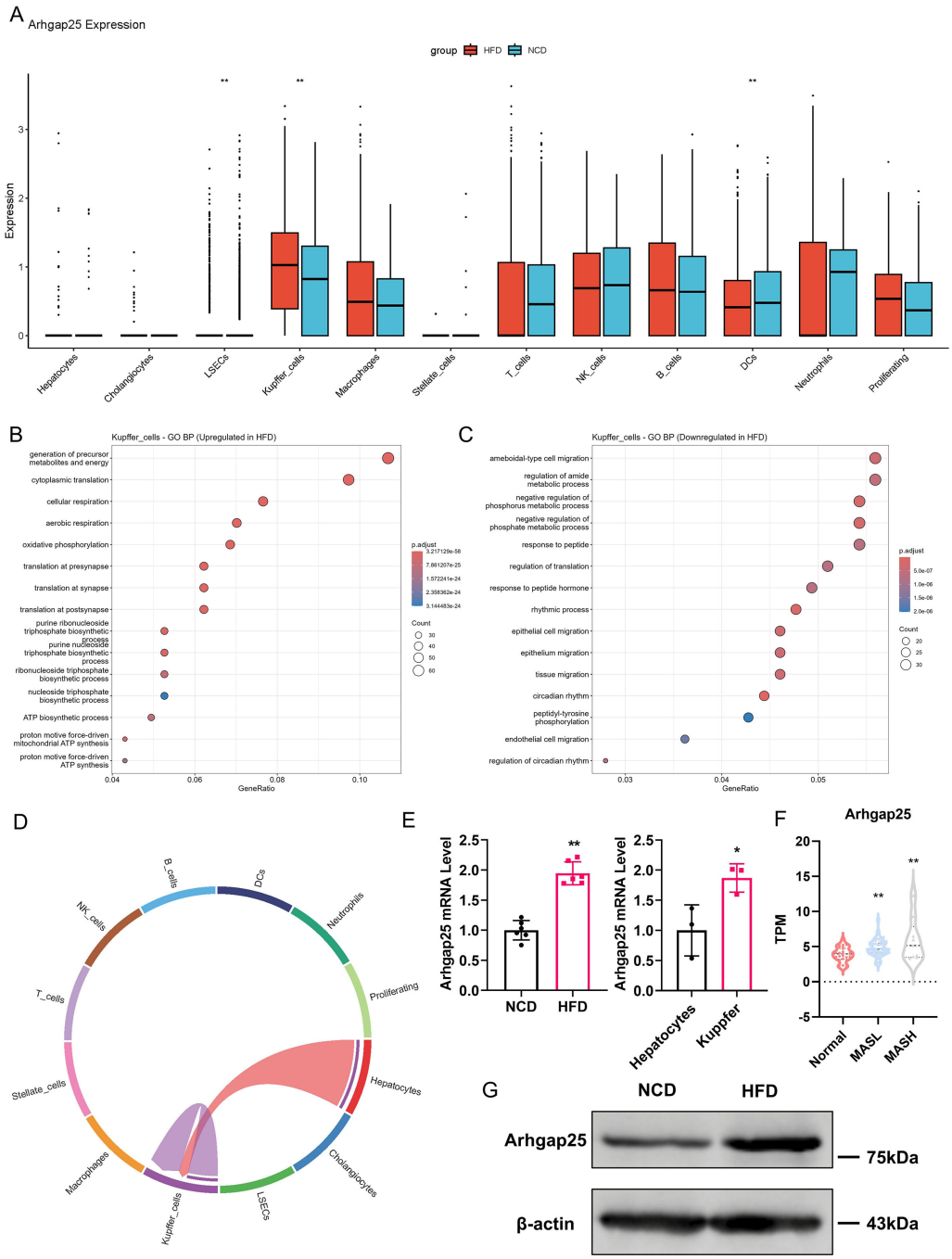

Fig. 2. Validation of *Arhgap25* expression and functional analysis in KCs. (A) Distribution of *Arhgap25* expression across various cell types in the HFD and NCD groups. Significant upregulation is observed in KCs. (B,C) Top Gene Ontology biological processes enriched for genes significantly upregulated (B) and downregulated (C) in KCs under HFD conditions. (D) Chord diagram visualizing intercellular communication pathways between KCs and other hepatic cell populations. (E) Relative *Arhgap25* mRNA levels in HFD vs. NCD liver tissues (left) and in isolated hepatocytes vs. KCs (right). (F) TPM expression values for ARHGAP25 in the GSE281797 human fatty liver dataset. (G) Western blot analysis of Arhgap25 protein levels in NCD and HFD liver tissues, with β-actin serving as the internal control. Data in bar graphs are presented as the mean ± SEM. Statistical significance: $*p < 0.05$, $**p < 0.01$.

assays demonstrated that hepatic TG and TC concentrations were significantly elevated in the OE cohort ($p < 0.01$; Fig. 3C). Furthermore, serum levels of hepatocellular injury markers aspartate aminotransferase (AST) and alanine aminotransferase (ALT) were significantly elevated in the OE group relative to the NC group ($p < 0.01$; Fig. 3D), indi-

cating exacerbated hepatic damage. Concurrently, the successful overexpression of the target gene, *Arhgap25*, was confirmed both at the transcriptional level, with a significant increase in its mRNA expression in liver tissues ($p < 0.01$; Fig. 3E), and at the translational level, as evidenced by enhanced Arhgap25 protein expression in western blot analysis (Fig. 3G). Additionally, cell-type-specific analysis indicated that *Arhgap25* mRNA levels were significantly higher in KCs compared to primary hepatocytes ($p < 0.05$; Fig. 3F).

3.4 Arhgap25 Overexpression Induces Pro-inflammatory Cytokine Release and Promotes M1 Macrophage Polarization

To evaluate the impact of Arhgap25 on hepatic inflammation and macrophage infiltration, histological and molecular analyses were conducted. The OE group exhibited a marked pro-inflammatory state, characterized by significantly upregulated relative mRNA expression of key cytokines, including *MCP-1* and *TNF-α* ($p < 0.01$), and *IL-6* ($p < 0.05$), alongside elevated macrophage markers *ADGRE1* ($p < 0.01$) and *CD68* ($p < 0.05$) compared to the NC group (Fig. 4A). This inflammatory profile was consistent with systemic measurements, which revealed significantly elevated protein concentrations of IL-6 and TNF-α ($p < 0.01$; Fig. 4B), as well as increased serum free fatty acid (FFA) levels in the OE cohort ($p < 0.01$; Fig. 4E). Furthermore, immunofluorescence staining for the macrophage marker ADGRE1 demonstrated a substantial accumulation of macrophages in the liver, quantitatively confirmed by a significant increase in the mean integrated density in the OE group ($p < 0.01$; Fig. 4C,D). To further characterize the specific phenotype of the recruited macrophages, we analyzed the expression profiles of M1 (classical, pro-inflammatory) and M2 (alternative, anti-inflammatory) polarization markers. *Arhgap25* overexpression induced a clear phenotypic shift toward M1 polarization. Specifically, the relative mRNA expression levels of the M1 markers *ITGAX* and *IL-1β*, along with the general macrophage marker *F4/80*, were significantly upregulated in the OE group ($p < 0.01$). Conversely, the expression of the M2-associated markers *ARG1* ($p < 0.05$) and *FIZZ1* ($p < 0.01$) were significantly suppressed compared to NC controls (Fig. 4F). These transcriptional alterations were corroborated at the translational level via Western blot analysis, which revealed a distinct reduction in ARG1 protein levels coupled with concurrent increases in the pro-inflammatory proteins TNFα and IL1β in the OE group (Fig. 4G).

3.5 Activation of AKT/mTOR Signaling Exacerbates Arhgap25-Induced Lipid Accumulation and Inflammatory Responses In Vitro

Although systemic AAV transduces multiple hepatic cell types, our scRNA-seq analysis demonstrated that endogenous Arhgap25 expression is predominantly enriched in Kupffer cells, supporting KCs as the principal cellular target investigated in this study. To investigate the cellular effects of Arhgap25, we simulated the *in vivo* environment by pre-transducing Kupffer cells with AAV-Arhgap25 to overexpress the protein. Subsequently, under palmitic acid (PA) stimulation, we employed an *in vitro* co-culture model consisting of HepG2 hepatocytes and KC cells (Fig. 5A), with successful Arhgap25 protein overexpression confirmed via Western blot (Fig. 5B). Functionally, Arhgap25 overexpression significantly elevated extracellular FFA concentrations compared to the PBS control ($p < 0.01$; Fig. 5C) and markedly exacerbated intracellular lipid droplet accumulation, as evidenced by histological staining in the PA+Arhgap25 group relative to the PA-only group (Fig. 5D). This enhanced steatotic phenotype was supported at the molecular level by significant upregulation in the mRNA and protein expression of key adipogenic regulators, specifically PPARγ ($p < 0.01$), C/EBPβ ($p < 0.05$), and FABP4 ($p < 0.01$), while the lipolytic markers such as ATGL and HSL showed no significant alterations (Fig. 5F,G). Concurrently, Arhgap25 promoted a robust pro-inflammatory microenvironment, demonstrated by the elevated protein levels of the macrophage marker CD68 and the primary pro-inflammatory cytokines TNFα and IL-6 (Fig. 5E).

To further elucidate the underlying molecular mechanisms driving these lipid metabolic and inflammatory alterations, the AKT/mTOR intracellular signaling cascade was evaluated. Western blot analysis revealed that Arhgap25 overexpression substantially enhanced the phosphorylation levels of both AKT (p-AKT) and mTOR (p-mTOR) compared to the PBS control, without altering the baseline expression of total AKT and mTOR proteins (Fig. 5H). To validate the involvement of this pathway, an AKT inhibitor (AKT-IN) was introduced. Treatment with the inhibitor alone or in combination with Arhgap25 overexpression confirmed the specific modulation of p-AKT downstream of Arhgap25 (Fig. 5I). Collectively, these biochemical evaluations indicate that Arhgap25 mediates its pro-lipogenic and pro-inflammatory effects by promote the AKT/mTOR signaling axis.

4. Discussion

The onset and progression of MASLD are complex processes driven synergistically by hepatic lipid metabolic dysregulation and immune microenvironment disruption [22,23,24,25]. This study identifies Arhgap25 as a critical regulatory factor in the pathological progression of HFD-induced MASLD. Through multi-omics data mining, an *in vivo* AAV-mediated overexpression model, and an *in vitro* co-culture system, we demonstrated that Arhgap25 is specifically enriched in KCs. By promote the AKT/mTOR signaling pathway, Arhgap25 promotes the polarization of KCs toward a pro-inflammatory M1 phenotype, thereby exacerbating hepatocellular lipid accumulation and liver dysfunction. These findings not only broaden our under-

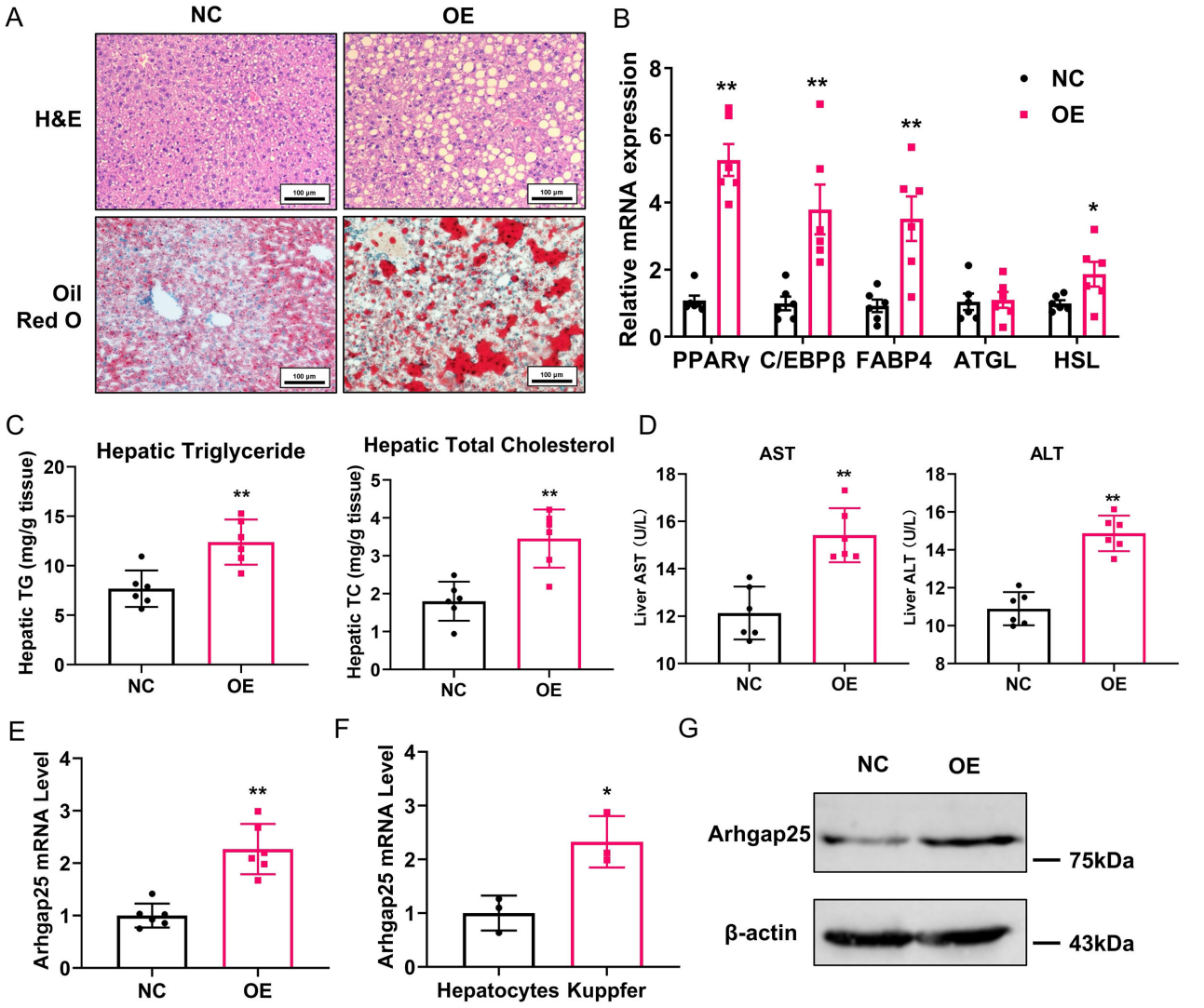

Fig. 3. *Arhgap25* promotes hepatic lipid accumulation *in vivo*. (A) Representative micrographs of liver tissues from AAV-mediated *Arhgap25* OE mice and NC mice. H&E staining (top row) reveals substantial macrovesicular steatosis in the OE group. Oil Red O staining (bottom row) shows increased lipid droplet deposition in OE liver tissues. Scale bars: 100 μm. (B) Relative hepatic mRNA expression of adipogenic genes (*PPARγ*, *C/EBPβ*, *FABP4*) and lipolytic genes (*ATGL*, *HSL*) in the NC and OE groups. (C) Quantitative biochemical analysis of hepatic TG and TC levels. (D) Quantitative analysis of AST and ALT in serum. (E) Confirmation of hepatic *Arhgap25* mRNA overexpression level in OE mice. (F) Cell-type-specific mRNA expression analysis comparing *Arhgap25* levels in primary hepatocytes and KCs. (G) Western blot analysis confirming Arhgap25 protein overexpression, with β-actin serving as the loading control. Data in bar graphs are presented as the mean ± SEM. Statistical significance: $*p < 0.05$, $**p < 0.01$.

standing of the mechanisms underlying hepatic immune-metabolic remodeling but also provide a promising molecular target for therapeutic interventions in MASLD.

Previous efforts to identify therapeutic targets for MASLD have often focused predominantly on the metabolic reprogramming of hepatic parenchymal cells themselves, while neglecting the core role of the immune microenvironment during disease initiation. Our integrative analysis of bulk and scRNA-seq robustly addresses this limitation, revealing that the HFD-induced transcriptional response is largely driven by myeloid-mediated inflammation. Specifically, under HFD-induced stress, the proportions of KCs and T cells in the liver increased significantly, with Arhgap25 being highly enriched within the KC population. This global shift in cellular composition suggests that the remodeling of the hepatic microenvironment accompanies, or perhaps even precedes, the onset of severe lipotoxicity. Cell-cell communication analysis further underscores the role of KCs as a central mediator linking inflammation to hepatocellular injury. Because Arhgap25 functions as a Rho GTPase-activating protein, its aberrant upregulation under metabolic stress

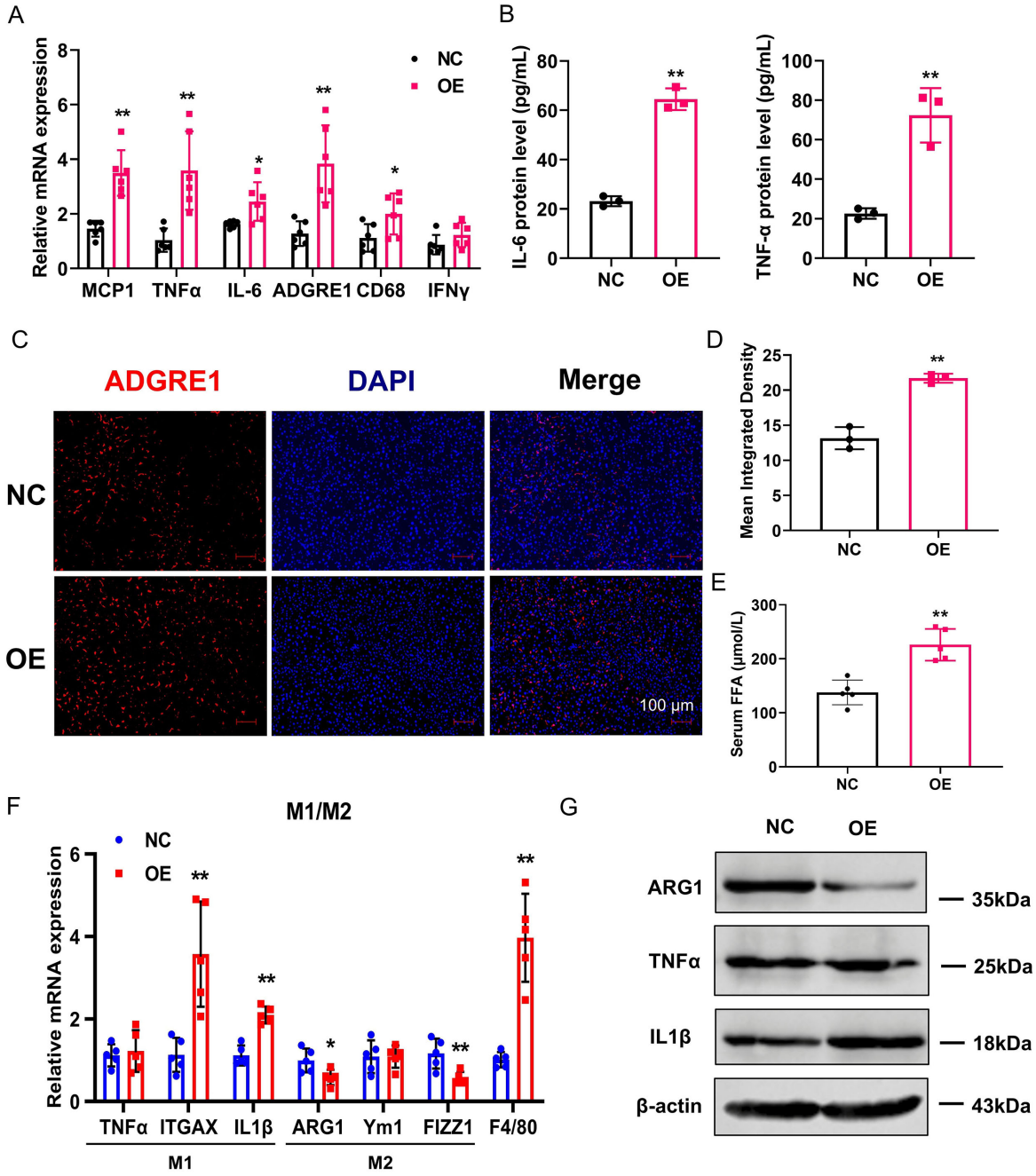

Fig. 4. Arhgap25 overexpression promotes hepatic inflammation and M1 macrophage polarization. (A) Relative hepatic mRNA expression levels of pro-inflammatory cytokines (*MCP1*, *TNFα*, *IL-6*) and macrophage markers (*ADGRE1*, *CD68*, *IFNγ*) in the NC and OE groups, measured by qPCR. (B) Systemic protein concentrations of IL-6 and TNFα in the serum of the NC and OE groups, determined via ELISA. (C) Representative immunofluorescence micrographs of liver tissues from the NC and OE groups. Sections were stained for the macrophage marker ADGRE1 (red) and counterstained with DAPI (blue). Scale bars: 100 μm. (D) Quantitative analysis of ADGRE1 staining intensity, presented as the mean integrated density. (E) Serum FFA concentrations in the NC and OE groups. (F) Relative hepatic mRNA expression levels of classical pro-inflammatory (M1) macrophage markers (*TNFα*, *ITGAX*, *IL1β*), alternative anti-inflammatory (M2) markers (*ARG1*, *Ym1*, *FIZZ1*), and the pan-macrophage marker *F4/80* in NC and OE groups. (G) Representative Western blot analysis of ARG1, TNFα, and IL1β protein levels in hepatic tissues from the NC and OE groups. β-actin was used as the loading control. Data in bar graphs are presented as the mean ± SEM. Statistical significance: $*p < 0.05$, $**p < 0.01$ compared to the NC group.

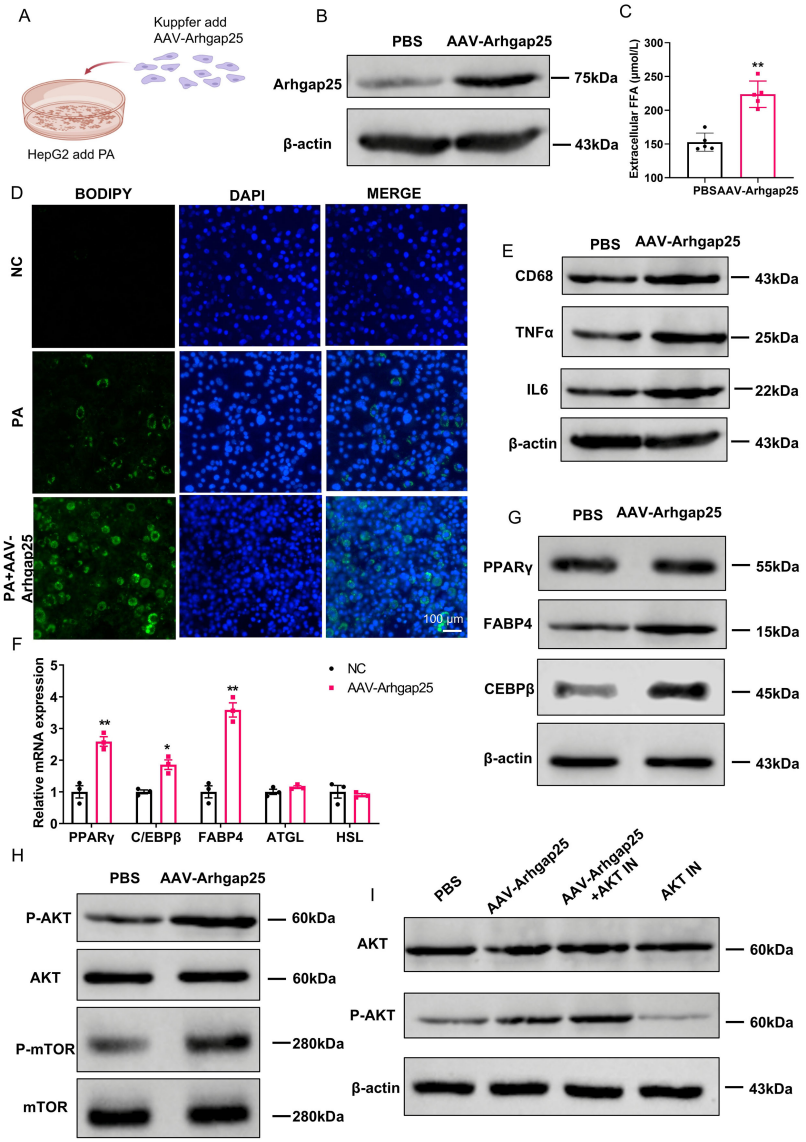

Fig. 5. *Arhgap25* exacerbates lipid accumulation and inflammatory responses *in vitro* via promoting of the AKT/mTOR signaling pathway. (A) Schematic diagram of the *in vitro* experimental design. HepG2 hepatocytes were stimulated with PA and co-cultured with Kupffer cells treated with PBS or transduced with AAV-Arhgap25. (B) Western blot analysis confirming successful Arhgap25 protein overexpression in KCs. β-actin served as a loading control. (C) *Arhgap25* overexpression significantly elevated concentrations of extracellular FFAs compared to the PBS control. (D) Representative micrographs of BODIPY staining of HepG2 cells under NC, PA, and PA+Arhgap25 conditions. Arhgap25 drastically exacerbated intracellular lipid droplet deposition (green staining) relative to the PA-only group. Scale bar: 100 μm. (E) Western blot analysis showing elevated protein levels of the macrophage marker CD68 and primary pro-inflammatory cytokines TNFα and IL-6 upon Arhgap25 overexpression in the co-culture system. β-actin was used as a loading control. (F) Relative mRNA expression levels of adipogenic genes (*PPARγ*, *C/EBPβ*, *FABP4*) and lipolytic genes (*ATGL*, *HSL*) in the NC and OE groups. Values are normalized to the NC group. (G) Representative Western blots of the adipogenic regulators PPARγ, FABP4, and C/EBPβ protein expression in the PBS and Arhgap25 OE groups. Molecular weights are given. β-actin served as a loading control. (H) Western blot evaluation of the AKT/mTOR signaling pathway. (I) Validation of pathway involvement using an AKT inhibitor (AKT-IN). Western blot analysis confirms the specific modulation of p-AKT downstream of Arhgap25 under various treatment conditions, including combination of Arhgap25 protein overexpression and AKT inhibitor (AKT-IN). Molecular weights are indicated. For all blots, β-actin served as the loading control. Data in bar graphs are presented as the mean ± SEM. Statistical significance: $*p < 0.05$, $**p < 0.01$ compared to the NC group.

likely rewires immune cell dynamics and activation capacity, elucidating why extensive macrophage infiltration (e.g., increased ADGRE1 expression) and a systemic burst of pro-inflammatory cytokines were observed in the Arhgap25 overexpression model.

Lipid metabolic dysregulation and inflammatory cascades are not isolated pathological events but are intricately intertwined through microenvironmental crosstalk [26,27,28]. Our functional experiments explicitly indicate that Arhgap25 overexpression not only drives the polarization of macrophages toward a classical pro-inflammatory M1 phenotype (characterized by elevated *ITGAX* and *IL1*β expression, alongside *ARG1* suppression) but also concurrently triggers the significant activation of adipogenic transcription factors (*PPARγ*, *C/EBPβ*) and severe hepatic macrovesicular steatosis. Mechanistically, this study reveals that Arhgap25 exerts these dual pathogenic effects by positively regulating the AKT/mTOR signaling axis. The AKT/mTOR pathway is a central signaling node that maintains cellular metabolic homeostasis and immune tolerance. The significant promoting of AKT/mTOR phosphorylation by Arhgap25 not only disrupts the balance of polarization signals within macrophages but also exacerbates the uptake of FFA and lipid droplet accumulation in hepatocytes within the co-culture system through paracrine signaling, driven by the robust secretion of cytokines (such as TNFα and IL-6). This pathologically deteriorating KCs-hepatocyte communication loop precisely elucidates the core driver role of Arhgap25 in driving liver injury (as manifested by significantly elevated serum AST and ALT levels).

Although this study provides substantial multidimensional evidence for the mechanistic role of Arhgap25 in MASLD, certain limitations warrant further investigation. First, the *in vivo* mechanistic validation in this study primarily relied on an AAV-mediated overexpression model; employing a hepatic macrophage-specific Arhgap25 conditional knockout (cKO) mouse model in future studies will enable a more definitive evaluation of the therapeutic safety and rescue efficacy of targeting this gene. Second, the direct interacting proteins or upstream epigenetic regulatory mechanisms through which Arhgap25 promote the AKT/mTOR pathway remain incompletely defined, necessitating further proteomics approaches to decipher its precise structural biological basis. Finally, as the data in this study were predominantly derived from rodent models and *in vitro* cell lines, future investigations should expand to large-scale human MASLD/NASH clinical cohorts to validate the clinical relevance of ARHGAP25 expression levels across different stages of liver fibrosis in human patients. Although Arhgap25 has been primarily characterized as a Rac-specific Rho GTPase-activating protein, accumulating evidence suggests that Rac signaling is closely interconnected with the PI3K/AKT/mTOR pathway [17,29]. Rac1 has been reported to regulate PI3K activation and subsequently promote AKT phosphorylation and mTOR signaling, thereby modulating inflammatory responses, cell survival, and metabolic homeostasis [29]. Conversely, inhibition of Rac activity attenuates PI3K/AKT signaling and suppresses downstream mTOR activation, leading to profound alterations in cellular metabolism and immune function. As a Rac-specific GAP, Arhgap25 accelerates the hydrolysis of GTP-bound Rac1 and thereby negatively regulates Rac activation [30]. Therefore, it is biologically plausible that Arhgap25 indirectly promote AKT/mTOR signaling through the inhibition of Rac activity. Supporting this notion, Huang et al. [17] demonstrated that ARHGAP25 inhibits pancreatic adenocarcinoma progression by suppressing glycolysis via the AKT/mTOR signaling pathway, suggesting that this protein is functionally linked to AKT signaling beyond its canonical regulation of Rac. Nevertheless, the molecular connection between Rac inactivation and AKT/mTOR suppression in KCs remains incompletely understood. In the present study, Arhgap25 overexpression was consistently associated with exaltation phosphorylation of AKT and mTOR. However, Rac activity was not directly evaluated; therefore, the precise signaling hierarchy remains to be established. It is possible that Arhgap25 promote AKT/mTOR signaling through Rac-dependent mechanisms or via additional interacting proteins involved in immune-metabolic regulation. Future studies employing Rac-GTP pull-down assays, constitutively active Rac1 rescue experiments, and PI3K/AKT activity assays will be valuable for clarifying the upstream regulatory events linking Arhgap25 to AKT/mTOR signaling in MASLD.

In conclusion, this study establishes Arhgap25 as a pivotal molecular mediator driving the pathological progression of MASLD. Arhgap25 upregulation in KCs promote the AKT/mTOR signaling pathway, which not only provokes a robust M1-type inflammatory response but also exacerbates parenchymal lipid accumulation and tissue injury via microenvironmental crosstalk. Targeted intervention against Arhgap25 or the immune-metabolic crosstalk network it mediates holds promise as an innovative therapeutic strategy to halt the progression from isolated steatosis to advanced steatohepatitis.

5. Limitations

Despite the strengths of our integrated transcriptomic analysis and experimental validation, several limitations should be acknowledged. First, the *in vivo* study relied on systemic AAV-mediated overexpression, which demonstrates the pathogenic effect of increased Arhgap25 expression but does not establish the requirement of endogenous Arhgap25 in MASLD progression. Future studies using KC-specific knockout or knockdown models are warranted. Second, although our scRNA-seq data identified Arhgap25 as being predominantly enriched in KCs, systemic AAV delivery is not cell-type-specific, and direct effects on other hepatic cell populations cannot be completely excluded. Finally, although we validated the upreg-

ulation of ARHGAP25 in public human MASLD transcriptomic datasets, additional studies using well-characterized clinical cohorts and mechanistic experiments—particularly those investigating the Rac-AKT/mTOR signaling axis—will be necessary to further define the cell-type-specific functions and translational potential of this protein in MASLD.

6. Conclusion

In conclusion, this study identifies Arhgap25 as a potential regulator of hepatic immune-metabolic remodeling during MASLD progression. Through integrated transcriptomic analyses, single-cell RNA sequencing, *in vivo* AAV-mediated overexpression, and *in vitro* co-culture experiments, we demonstrate that elevated Arhgap25 expression is predominantly associated with KCs and promotes pro-inflammatory macrophage polarization, hepatic lipid accumulation, and liver injury. Mechanistically, our findings suggest that these pathological effects are mediated by the acceleration of the AKT/mTOR signaling pathway, highlighting a potential molecular link between Arhgap25-mediated immune activation and metabolic dysregulation. Furthermore, validation using public human MASLD transcriptomic datasets supports the clinical relevance of increased ARHGAP25 expression. Although additional studies employing cell-type-specific loss-of-function models are required to establish causality and define the precise signaling mechanisms, our findings provide new insights into the role of Arhgap25 in MASLD and suggest that the modulation of Arhgap25-dependent immune-metabolic crosstalk may represent a promising therapeutic strategy for preventing disease progression.

Availability of Data and Materials

All raw data can be obtained by contacting the corresponding author.

Author Contributions

YW: Conceptualization, Data curation, Investigation, Methodology, Writing–original draft, Visualization; SSL: Writing–review and editing, Project administration, Supervision, Conceptualization, Funding Acquisition, Visualization. Both authors contributed to editorial changes in the manuscript. Both authors read and approved the final manuscript. Both authors have participated sufficiently in the work and agreed to be accountable for all aspects of the work.

Ethics Approval and Consent to Participate

All animal protocols were approved by the Laboratory Animal Administration Committee of Zhengzhou University. The experiments were conducted in strict accordance with the Guidelines for Animal Experimentation of School of Basic Medical Sciences, Zhengzhou University (SQ 2026-2380). All animal experiments complied with relevant regulations regarding animal welfare in China and the policies of Zhengzhou University concerning animal experimentation.

Acknowledgment

Not applicable.

Funding

We thank the Henan Provincial Natural Science Foundation General Program (262300421625) for funding this study.

Conflicts of Interest

The authors declare no conflicts of interest.

Supplementary Material

Supplementary material associated with this article can be found, in the online version, at https://doi.org/10.31083/FBL53591.

References

[1] Kendall TJ, Jimenez-Ramos M, Turner F, Ramachandran P, Minnier J, McColgan MD, et al. An integrated gene-to-outcome multimodal database for metabolic dysfunction-associated steatotic liver disease. Nature Medicine. 2023; 29: 2939–2953. https://doi.org/10.1038/s41591-023-02602-2

[2] Yu X, Huang C, Evers M, Liu J, Ting HJ, Zhang S, et al. Targeted inhibition of hepatic de novo ceramide synthesis ameliorates MASH. Science Advances. 2025; 11: eadx2681. https://doi.org/10.1126/sciadv.adx2681

[3] Meng L, Lu F, Zhang B, Ma Y, Gao J. Taming fatty liver: can taurine combat metabolic dysfunction in MASLD? Cell Communication and Signaling : CCS. 2025; 23: 439. https://doi.org/10.1186/s12964-025-02439-x

[4] Martin-Grau M, Monleón D. The Role of Microbiota-Related Co-Metabolites in MASLD Progression: A Narrative Review. Current Issues in Molecular Biology. 2024; 46: 6377–6389. https://doi.org/10.3390/cimb46070381

[5] Jeong BK, Choi WI, Choi W, Moon J, Lee WH, Choi C, et al. A male mouse model for metabolic dysfunction-associated steatotic liver disease and hepatocellular carcinoma. Nature Communications. 2024; 15: 6506. https://doi.org/10.1038/s41467-024-50660-y

[6] Cui J, Lin Z, Sun M, He Y, Mao Y, Zhang C, et al. Intracellular IL-24 ameliorates lipid metabolic disorders in metabolic dysfunction-associated steatohepatitis by restoring the autophagy-lysosome pathway. Cellular and Molecular Life Sciences : CMLS. 2025; 82: 417. https://doi.org/10.1007/s00018-025-05940-1

[7] Miyazaki H, Kinoshita M, Nakashima H, Nakamura S, Saitoh D. Pioglitazone Modifies Kupffer Cell Function and Protects against *Escherichia coli*-Induced Bacteremia in Burned Mice. International Journal of Molecular Sciences. 2022; 23: 12746. https://doi.org/10.3390/ijms232112746

[8] Tan J, Zhang J, Wang M, Wang Y, Dong M, Ma X, et al. DRAM1 increases the secretion of PKM2-enriched EVs from hepatocytes to promote macrophage activation and disease progression in ALD. Molecular Therapy. Nucleic Acids. 2021; 27: 375–389. https://doi.org/10.1016/j.omtn.2021.12.017

[9] Dong T, Hu G, Fan Z, Wang H, Gao Y, Wang S, et al. Activation of GPR3-β-arrestin2-PKM2 pathway in Kupffer cells stimulates glycolysis and inhibits obesity and liver pathogenesis. Nature Communications. 2024; 15: 807. https://doi.org/10.1038/s41467-024-45167-5

[10] Chan MM, Daemen S, Beatty W, Byrnes K, Cho K, Ferguson D, et al. Induction of TFEB promotes Kupffer cell survival and reduces lipid accumulation in MASLD. Hepatology Communications. 2025; 9: e0853. https://doi.org/10.1097/hc9.0000000000000853

[11] Elnagdy M, Barve S, McClain C, Gobejishvili L. cAMP Signaling in Pathobiology of Alcohol Associated Liver Disease. Biomolecules. 2020; 10: 1433. https://doi.org/10.3390/biom10101433

[12] Duan Y, Pan X, Luo J, Xiao X, Li J, Bestman PL, et al. Association of Inflammatory Cytokines With Non-Alcoholic Fatty Liver Disease. Frontiers in Immunology. 2022; 13: 880298. https://doi.org/10.3389/fimmu.2022.880298

[13] Braunersreuther V, Viviani GL, Mach F, Montecucco F. Role of cytokines and chemokines in non-alcoholic fatty liver disease. World Journal of Gastroenterology. 2012; 18: 727–735. https://doi.org/10.3748/wjg.v18.i8.727

[14] Sasvári P, Pettkó-Szandtner A, Wisniewski É, Csépányi-Kömi R. Neutrophil-specific interactome of ARHGAP25 reveals novel partners and regulatory insights. Scientific Reports. 2024; 14: 20106. https://doi.org/10.1038/s41598-024-71002-4

[15] Wisniewski É, Czárán D, Kovács F, Bahurek E, Németh A, Sasvári P, et al. A novel BRET-Based GAP assay reveals phosphorylation-dependent regulation of the RAC-specific GTPase activating protein ARHGAP25. FASEB Journal : Official Publication of the Federation of American Societies for Experimental Biology. 2022; 36: e22584. https://doi.org/10.1096/fj.202200689R

[16] Csépányi-Kömi R, Sirokmány G, Geiszt M, Ligeti E. ARHGAP25, a novel Rac GTPase-activating protein, regulates phagocytosis in human neutrophilic granulocytes. Blood. 2012; 119: 573–582. https://doi.org/10.1182/blood-2010-12-324053

[17] Huang WK, Chen Y, Su H, Chen TY, Gao J, Liu Y, et al. ARHGAP25 Inhibits Pancreatic Adenocarcinoma Growth by Suppressing Glycolysis via AKT/mTOR Pathway. International Journal of Biological Sciences. 2021; 17: 1808–1820. https://doi.org/10.7150/ijbs.55919

[18] Csépányi-Kömi R, Wisniewski É, Bartos B, Lévai P, Németh T, Balázs B, et al. Rac GTPase Activating Protein ARHGAP25 Regulates Leukocyte Transendothelial Migration in Mice. Journal of Immunology (Baltimore, Md. : 1950). 2016; 197: 2807–2815. https://doi.org/10.4049/jimmunol.1502342

[19] Ribas V, Morón-Ros S, Marí H, Gracia-Batllori A, Brugnara L, Herrero-Gómez A, et al. Diet-induced obesity disrupts sexually dimorphic gene expression in mice. American Journal of Physiology. Cell Physiology. 2025; 329: C987–C1003. https://doi.org/10.1152/ajpcell.00098.2025

[20] Wu Z, Wang Z, Chang X, Chen X, Ding Q, Fu R, et al. Prioritizing pathway signature using deep learning approach: a novel strategy for traditional Chinese medicine formula generation and optimization. Briefings in Bioinformatics. 2025; 26: bbaf403. https://doi.org/10.1093/bib/bbaf403

[21] Iwata A, Maruyama J, Natsuki S, Nishiyama A, Tamura T, Tanaka M, et al. Egr2 drives the differentiation of Ly6C^{hi} monocytes into fibrosis-promoting macrophages in metabolic dysfunction-associated steatohepatitis in mice. Communications Biology. 2024; 7: 681. https://doi.org/10.1038/s42003-024-06357-5

[22] Steinberg GR, Valvano CM, De Nardo W, Watt MJ. Integrative metabolism in MASLD and MASH: Pathophysiology and emerging mechanisms. Journal of Hepatology. 2025; 83: 584–595. https://doi.org/10.1016/j.jhep.2025.02.033

[23] Syed-Abdul MM. Lipid Metabolism in Metabolic-Associated Steatotic Liver Disease (MASLD). Metabolites. 2023; 14: 12. https://doi.org/10.3390/metabo14010012

[24] Jin J, Cheng K, Chen M, Liang H, Zhang W. Immunotherapy resistance in MASLD-related hepatocellular carcinoma: special immune microenvironment and gut microbiota. International Journal of Biological Sciences. 2025; 21: 5666–5690. https://doi.org/10.7150/ijbs.117394

[25] Zhao H, Wang W, Zhu P, Shi Z. Macrophage-tregs crosstalk: the “hub” of the immune network in MASLD. Frontiers in Immunology. 2025; 16: 1680878. https://doi.org/10.3389/fimmu.2025.1680878

[26] Reue K, Wang H. Mammalian lipin phosphatidic acid phosphatases in lipid synthesis and beyond: metabolic and inflammatory disorders. Journal of Lipid Research. 2019; 60: 728–733. https://doi.org/10.1194/jlr.S091769

[27] Saadati S, Godini R, Reddy A, Teede H, Mousa A. Metabolic crossroads in insulin resistance: exploring lipid dysregulation and inflammation. Frontiers in Immunology. 2025; 16: 1692742. https://doi.org/10.3389/fimmu.2025.1692742

[28] Xu S, Lu F, Gao J, Yuan Y. Inflammation-mediated metabolic regulation in adipose tissue. Obesity Reviews : an Official Journal of the International Association for the Study of Obesity. 2024; 25: e13724. https://doi.org/10.1111/obr.13724

[29] Saci A, Cantley LC, Carpenter CL. Rac1 regulates the activity of mTORC1 and mTORC2 and controls cellular size. Molecular Cell. 2011; 42: 50–61. https://doi.org/10.1016/j.molcel.2011.03.017

[30] Mäkitie RE, Henning P, Jiu Y, Kämpe A, Kogan K, Costantini A, et al. An *ARHGAP25* variant links aberrant Rac1 function to early-onset skeletal fragility. JBMR Plus. 2021; 5: e10509. https://doi.org/10.1002/jbm4.10509